

ROLE OF MULTI PARAMETRIC MRI IN THE EVALUATION OF MALIGNANT RENAL MASSES

Essay Submitted for partial fulfillment of Master degree of Radiodiagnosis

By

Ahmad Ibrahim Sayed

M.B., B.Ch.

Supervised By

Prof. Dr. Dalia Zaki Zidan

Assistant Professor of Radiodiagnosis
Faculty of Medicine
Ain Shams University

Dr. Aya Yassin Ahmed

Lecturer of Radiodiagnosis Faculty of Medicine Ain Shams University

Faculty of Medicine Ain Shams University

2013



دور التصوير باشعة الرنين المغناطيسي متعدد الأطوار في تقييم الكتل الكلويه السرطانية

رسالة

توطئة للحصول على درجة الماجستير في الأشعة التشخيصية

مقدمة من

الطبيب / أحمد إبراهيم سيد عبد الفتاح بكالوريوس الطب والجراحة

تحت إشراف

أ. د. دالیا زکی زیدان

أستاذ مساعد الأشعة التشخيصية كلية الطب جامعة عين شمس

د. آیه یاسین اُحمد

مدرس الأشعة التشخيصية كلية الطب جامعة عين شمس

كلية الطب

جامعة عين شمس

2013



- First, and foremost, all thanks and gratitude to GOD, most gracious and most merciful.
- I would like to express my deepest gratitude and sincere thanks to Prof. Dr.
 Dalia Zidan, for devoting much of her precious time, kind guidance and valuable advice for enriching this work.
- I am extremely grateful to **Dr. Aya Yassin**, for her continuous guidance and valuable suggestions, saving no effort or time to read every word in this work.

Contents

- I. List of Figures & Tables
- II. List of Abbreviations
- III. Introduction and aim of the work.
- IV. Anatomical considerations.
- V. Pathology of malignant renal masses.
- VI. MRI principles and technical considerations.
- VII. MRI findings in malignant renal masses.
- VIII. Summary and conclusion.
 - IX. References.
 - X. Arabic summary.

List Of Figures

Fig.	Title	Page number
Number		
Fig 1.1	Both kidneys in situ from anterior view	5
Fig 1.2	The anterior surfaces of the kidneys	6
Fig 1.3	Posterior relations of the kidney.	8
Fig 1.4	Peritoneal spaces at the level of the kidneys	10
Fig1.5	Right kidney sectioned in several planes	11
Fig1.6	The principal arteries and veins of a kidney	12
Fig1.7	A simplified illustration of blood flow and the	14
	venous drainage of the kidney	
Fig 1.8	T1W MRI through the kidney (a) Coronal view	16
	and (b) Sagital view.	
Fig1.9	T1-weighted inversion-recovery image of upper	17
	abdomen	
Fig1.10	Coronal T2-weighted single-shot fast spin-echo	17
	(SE) or half-Fourier single-shot turbo SE image	
	shows the kidneys	
Fig1.11	Normal renal enhancement patterns in a patient	20
	with a normal functioning kidney.	
Fig1.12	Importance of cine MR urography in	22
	demonstrating the entire ureters with static-fluid	
	techniques.	
Fig1.13	Excretory MRU; coronal MIP image shows a	24
	single unduplicated pelvicalyceal system and	
	ureters.	

		I
Fig1.14	Coronal MIP of a subtracted contrast-enhanced 3D MR urogram.	24
Fig 2.1	Putative sites of origin of RCC and NF-κB expression.	27
Fig 2.2	Gross specimen of a multilocular cystic RCC.	29
Fig2.3	Pseudocapsule formation in expansile growth.	30
Fig 2.4	Pathology specimen shows urothelial tumor of renal pelvis	36
Fig 2.5	Sarcoma at the lower pole of the left kidney	37
Fig 2.6	Renal Lymphoma (Hematoxylin and Eosin) ×	39
	30.	
Fig 3.1	Navigator-triggered T2-weighted turbo spin echo axial sequence.	49
Fig 3.2	Coronal Single-Shot TSE projection images	50
	without (a) and with parallel imaging.	
Fig 3.3	MR urography (MRU) in a patient with right	55
	ureteral carcinoma.	
Fig 3.4	Schematic illustration of the diffusion-weighted imaging sequence.	60
Fig 3.5	ADC map for normal values	69
Fig 3.6	Diffusion-weighted tensor image of the right	71
	kidney.	
Fig 4.1	stage 4 RCC	74
Fig 4.2	Coronal late arterial phase gadolinium-enhanced	75
	3D gradient-echo T1-weighted image	
	(heterogeneous tumor thrombus extending into	
	left renal vein).	
Fig 4.3	Renal cell carcinoma invading perinephric fat.	78
Fig 4.4	Clear cell renal cell carcinoma in a 65-year-old	83
	man.	
Fig 4.5	Multimodal presentation of a common type RCC.	84

Images in 46-year-old man with clear cell RCC.	85
Images in 28-year-old man with papillary RCC.	86
A 45-year-old man, papillary RCC (pT1b, G3) of	87
the right kidney.	
Images in 50-year-old woman with	88
chromophobic RCC.	
T1-weighted gradient echo images before (a) and	91
after (b) gadolinium administration of TCC.	
•	92
Transitional cell carcinoma in 81-year-old man.	93
Wilm's tumor in a 3-year-old boy with an abdominal mass.	95
(a) HASTE T2WI Coronal (b) BLADE T2WI	95
Axial (c) CE VIBE axial of wilms' tumor.	
Transverse short inversion time inversion-	96
recovery T2-weighted spin-echo MR image	
(5970/114/145) shows a left-sided abdominal	
mass with retroperitoneal lymphadenopathy.	
Non-Hodgkin follicular B-cell lymphoma in a	98
64-year-old man.	
Axial contrast-enhanced 2D T1-weighted GRE	98
and coronal contrast-enhanced 3D T1-weighted	
lymphoma.	
Monophasic renal synovial sarcoma in a 47-	99
year-old man.	
	Images in 28-year-old man with papillary RCC. A 45-year-old man, papillary RCC (pT1b, G3) of the right kidney. Images in 50-year-old woman with chromophobic RCC. T1-weighted gradient echo images before (a) and after (b) gadolinium administration of TCC. Renal pelvis transitional cell carcinoma. Transitional cell carcinoma in 81-year-old man. Wilm's tumor in a 3-year-old boy with an abdominal mass. (a) HASTE T2WI Coronal (b) BLADE T2WI Axial (c) CE VIBE axial of wilms' tumor. Transverse short inversion time inversion-recovery T2-weighted spin-echo MR image (5970/114/145) shows a left-sided abdominal mass with retroperitoneal lymphadenopathy. Non-Hodgkin follicular B-cell lymphoma in a 64-year-old man. Axial contrast-enhanced 2D T1-weighted GRE and coronal contrast-enhanced 3D T1-weighted GRE MR Image of B-cell non-Hodgkin lymphoma. Monophasic renal synovial sarcoma in a 47-

List of Tables

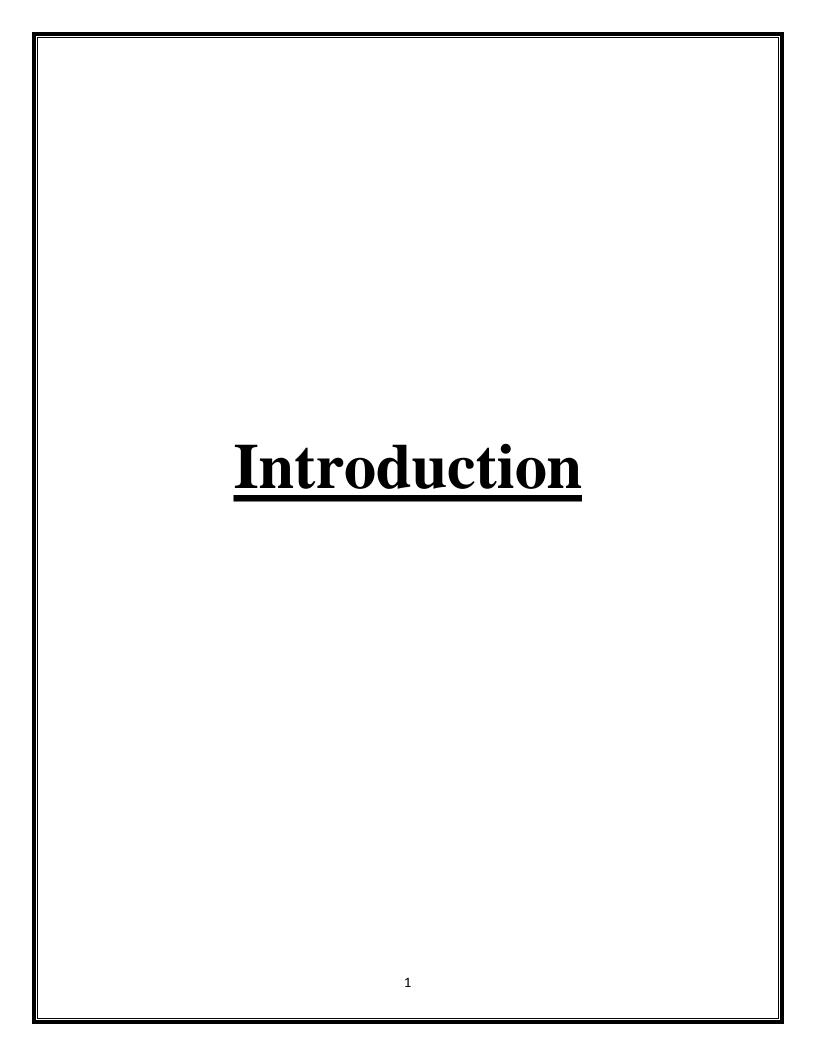
Table	Title	Page number
number		
Table2.1	TNM staging system for kidney.	31
Table 2.2	Wilm's most common staging system.	35
Table 3.1	Commonly used diffusion-weighted sequences for evaluating extra-cranial malignancy.	63
Table 3.2	Interpretation guidelines for DW-MRI.	66
Table3.3	Overview of <i>b</i> Values and Corresponding ADCs of Normal Kidneys as Reported in the Literature.	68
Table 3.4	Summary of renal MRI imaging protocol.	71

List of Abbreviations

3D FSPGR	three dimensional fast spoiled gradient echo
3D MR	Three Dimensional Magnetic Resonance
3T	Three Tesla
ADC	Apparent Diffusion Coefficient
CDC	Collecting Duct Carcinoma
CT	Computed Tomography
ccRCC	clear cell renal cell carcinoma
DCE MR	Dynamic Contrast Medium Enhanced
	Magnetic Resonance
DTI	diffusion-tensor imaging
DWI	Diffusion Weighted Imaging
EPI	echoplanar imaging
ESRD	End-Stage Renal Disease
ERCP	Endoscopic Retrograde
	Cholangiopancreatography
FLASH	Fast Low Angle Shot
FFE	Fast Field Echo
FISP	Fast Imaging with Steady state Precession
	renal disease
Gd	Gadolinium
GRE	gradient echo
GI	Gastrointestinal
GFR	Glomerular Filtration Rate
H&E	hematoxylin-eosin
HASTE	Half Fourier single-shot turbo spin echo
	sequence
ISSs	integrated staging systems
IVC	Inferior Vena Cava

IVU	Intravenous Urography
MIP	Maximum Intensity Projection
Msec	Millie second
MRU	Magnetic Resonance Urography
MT	Magnetization Transfer
MRI	Magnetic Resonance Imaging
MRCP	Magnetic Resonance
	Cholangiopancreatography
NSF	Nephrogenic systemic fibrosis
NFD	nephrogenic fibrosing dermopathy
NK-κB	nuclear factor kappa B
PRL	primary renal lymphoma
PSIF	The reversed FISP sequence
RF	Radiofrequency
RMC	Renal Medullary Carcinoma
RCC	Renal Cell Carcinoma.
RARE	Rapid Acquisition with Relaxation
	Enhancement
ROI	Area of Interest
SSTSE	Single shot turbo spin echo
SNR	signal-to-noise ratio
Sec	Second
SPAIR	SPectral Attenuated Inversion Recovery
STIR	Short TI Inversion Recovery
SE	Spin Echo
TSE	turbo spin echo
TCC	Transitional Cell Carcinoma
TNM	Primary tumor, lymphnode, metastases
TRs	short repetition times
UUT TCC	Upper Urothelial Tract Transitional Cell
	Carcinoma
VIBE	Volume Interpolated Body Examination
VR	Volume rendering

VHL	Von-Hippel Lindau	
	VIII	



Introduction

Globally there are over 200,000 new cases of renal cancer per year, with more than 100,000 deaths and the incidence is increasing at around 2% per year in Europe and North America [Woodward et al., 2011]. For 2011 it is estimated that about 61,000 new cases will be diagnosed and approximately 13,000 patients will die from this disease in the US [Siegel et al., 2011].

Renal cell carcinoma (RCC) accounts for 80–90% of all renal malignancies and the overall 5 year survival rate is approximately 45% [Szendroi et al., 2010].

Renal masses are a common finding in sectional imaging. Thus, distinguishing the different tumor types, such as clear cell renal cell carcinoma (ccRCC) and transitional cell carcinoma (TCC), is crucial for the decision-making process and determining the appropriate (interventional) therapy options. Functional magnetic resonance imaging lends hope of being able to facilitate differentiation between renal malignancies and benign lesions. In this regard, several studies have investigated different functional magnetic resonance (MR) techniques such as dynamic contrast mediumenhanced (DCE) MR, arterial spin labeling, MR spectroscopy, blood oxygen level-dependent MR, and diffusion-weighted MR imaging (DWI) [Palmowski et al., 2010] & [Thoeny and Keyzer, 2011].

By Diffusion weighted technique, T1 signal characteristics of a renal lesion appear to be related to the apparent diffusion coefficient (ADC) of the lesion.

ADC may be helpful in characterizing and differentiating renal masses [Zhang et al., 2009]. MR urography can also be used to evaluate the urinary tract and has the advantage of not using ionizing radiation and the potential to provide more functional information than CT [Silverman et al., 2009].

